Observation of robust energy transfer in the photosynthetic protein allophycocyanin using single-molecule pump-probe spectroscopy

Raymundo Moya
Massachusetts Institute of Technology
Audrey Norris
Massachusetts Institute of Technology
Toru Kondo
Tokyo Institute of Technology
Gabriela Schlau-Cohen (gssc@mit.edu)
Massachusetts Institute of Technology https://orcid.org/0000-0001-7746-2981

Article

Keywords: photoenergy transfers, photosynthetic organisms, light harvesting

Posted Date: March 12th, 2021

DOI: https://doi.org/10.21203/rs.3.rs-272109/v1

Version of Record: A version of this preprint was published at Nature Chemistry on January 6th, 2022.
See the published version at https://doi.org/10.1038/s41557-021-00841-9.

Observation of robust energy transfer in the photosynthetic protein allophycocyanin using single-molecule pump-probe spectroscopy

Raymundo Moya[1], Audrey C. Norris[1], Toru Kondo[2], Gabriela S. Schlau-Cohen[1*]

[1]Department of Chemistry, Massachusetts Institute of Technology,

77 Massachusetts Avenue, Cambridge, Massachusetts 02139, USA

[2]Department of Life Science and Technology, Tokyo Institute of Technology

*To whom correspondence should be addressed; E-mail: gssc@mit.edu

Abstract

Photosynthetic organisms convert sunlight to electricity with near unity quantum efficiency. Absorbed photoenergy transfers through a network of chromophores positioned within protein scaffolds, which fluctuate due to thermal motion. The resultant variation in energy transfer has not yet been measured, and so how the efficiency is robust to this variation, if any, has not been determined. Here, we describe single-molecule pump-probe spectroscopy with facile spectral tuning and its application to the ultrafast dynamics of single allophycocyanin, a light-harvesting protein from cyanobacteria. Using the spectral dependence of the dynamics, energy transfer and energetic relaxation from nuclear motion were disentangled. For energy transfer, an asymmetric distribution of timescales was observed. For energetic relaxation, the timescales were slower and more heterogeneous due to the impact of the protein environment. Collectively, these results suggest that energy transfer is robust to protein fluctuations, a prerequisite for efficient light harvesting.

Introduction

Photosynthetic light-harvesting systems power most life on earth by capturing and directing absorbed energy through networks of protein-scaffolded chromophores [1]. Rapid transfer of the absorbed energy is driven by coupling between the transition dipole moments of the chromophores. Fluctuations of the protein scaffold induce changes in the distances and orientations of the transition dipole moments that can, in turn, change the timescales of energy transfer [2–7]. Despite these fluctuations, energy travels through the light-harvesting systems to reach the reaction center with near-unity quantum efficiency [1, 8]. Heterogeneity in the timescales of energy transfer, *i.e*, the impact of protein fluctuations on light harvesting, has not yet been characterized.

Over the past decades, single-molecule methods have been a powerful approach to characterize heterogeneity in biological, chemical, and material systems, including photosynthetic light-harvesting proteins [9–12].More recently, single-molecule pump-probe spectroscopy (SM2P) emerged as a technique to resolve femtosecond processes, such as energy transfer. SM2P maps femtosecond dynamics onto fluorescence intensity using two ultrafast isoenergetic pulses to generate a pump-probe like excitation, where the temporal resolution is from the delay time between pulses (Fig. 1a) [13–16]. This technique has been applied to various ultrafast processes in single molecules, including coherent wavepacket oscillations and relaxation within the excitonic states of light-harvesting proteins from purple bacteria [16–18]. The complexity of the ultrafast dynamics of light-harvesting proteins has, however, obfuscated the heterogeneity specific to energy transfer. Furthermore, most of these measurements lacked spectral dependence, which provides an additional axis to help disentangle the contributions associated with each process.

The cyanobacterial light-harvesting protein, allophycocyanin (APC), contains strongly coupled dimers of chromophores that serve as a minimal system to examine photosynthetic energy transfer (Fig. 1b). Ensemble ultrafast measurements found complex kinetics of energy transfer within APC, potentially due to heterogeneous timescales [19–28]. Consistently, single-molecule fluorescence measurements identified heterogeneous photophysical states that arose from fluctuations of the protein scaffold [29–34], yet their impact on energy transfer could not be resolved due to the limited time resolution of fluorescence measurements.

Here, we report SM2P with facile spectral tuning across the visible region and perform SM2P measurements on APC, the homologous protein C-phycocyanin (CPC), and a chromophore in solution. Based on the spectral dependence of the dynamics and the concomitantly-measured fluorescence lifetimes, the distributions of energy relaxation and energy transfer timescales were separated for APC. The energy transfer timescales were centered at $\sim$150 fs. While the mean of the distribution agreed with the longer timescale from ensemble measurements, the median of the distribution was $\sim$100 fs shorter, suggesting that ensemble values may be lengthened due to slow sub-populations. The asymmetric nature of the distribution gives rise to non-mono-exponential behavior in the ensemble, such as the multi-exponential energy transfer observed in previous measurements [22, 28]. Broad distributions of energetic relaxation timescales were observed for both APC and CPC, which comparison to choromophores in solution indicated arises from the protein structure. Furthermore, slow energetic relaxation was observed in APC, enabling energy transfer to precede, and thus likely be unaffected by, the heterogeneity in the relaxation timescales. Together, these results demonstrate that rapid energy transfer is maintained despite fluctuations of the protein, which may play a role in the high quantum efficiency of photosynthetic light harvesting.

Results

Ultrafast dynamics in APC

We used SM2P to determine the distribution of ultrafast energetic relaxation timescales in APC. APC forms a trimer where each monomer contains two protein subunits, known as α and β, that each bind a phycocyanobilin chromophore, which are positioned on distal ends of the monomer ($\sim$5 nm apart) [35, 36]. The structural model of trimeric APC is shown in Fig. 1b. Upon trimerization, complementary chromophores on different monomers are brought close together ($\sim$2 nm apart) to generate the dimer shown in Fig. 1b, inset [35, 36]. The trimers assemble into the central core of the primary cyanobacterial light-harvesting structure, known as the phycobilisome [36]The linear absorption spectrum of APC is shown in Fig. 1c with the calculated absorption profiles for the underlying states [22]. The higher energy state has a broad absorption and the lower energy state has narrow absorption with a clear vibrational mode at $\sim$1,600 cm^{-1} above the primary transition. Although the electronic coupling between the α

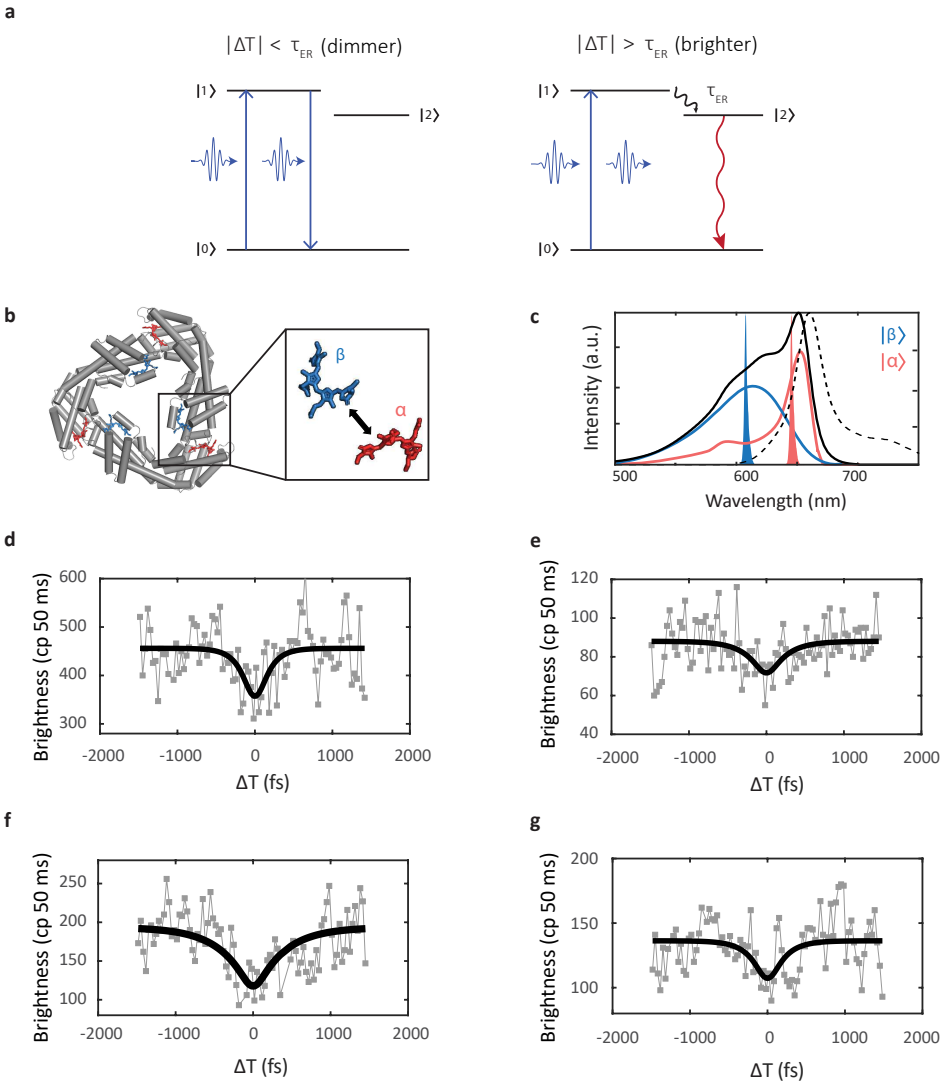

Figure 1: Single-molecule pump probe (SM2P) experiments on allophycocyanin: (**a**) Two laser pulses are focused onto the sample where energy relaxes between two excited states (a donor, $|1\rangle$, and an acceptor, $|2\rangle$) with a timescale, τ_{ER}. If ΔT is less than τ_{ER} (left), pulse 2 stimulates emission, decreasing the fluorescence intensity. If ΔT is greater than τ_{ER} (right), fluorescence emission occurs, increasing the fluorescence intensity. Scanning the time delay from negative to positive delays produces a dip like shape where the width of the modulation is governed by τ_{ER}. (**b**) Structural model of allophycocyanin with the β (blue) and α (red) chromophores (PDBID 1ALL). (**c**) Absorption (solid) and emission (dashed) spectra are shown with the 610 nm and 645 nm excitation in blue and red, respectively. The individual spectra for the α and β chromophores are shown in blue and red [22]. Representative SM2P traces (gray) of allophycocyanin with fits (black) for 610 nm excitation with decay time constants of 148$\pm$15 and 225$\pm$70 fs are shown in (**d**) and (**e**), respectively and for 645 nm excitation with decay time constants of 371$\pm$46 and 185$\pm$39 fs are shown in (**f**) and (**g**), respectively.

and β chromophores leads to excited states that are a linear combination of the excited states of the individual chromophores, the large energy gap means that the higher energy state is dominated by the β chromophore and the lower energy one by the α chromophore [19, 22]. Thus, here we refer to the states based on their dominant contribution.

The SM2P apparatus was constructed with a tunable excitation laser and a single-axis prism compressor to enable straightforward wavelength changes, which was used to investigate the dynamics of the individual chromophores. SM2P experiments on APC were performed with an excitation laser centered at 610 nm and 645 nm, which were selected to predominantly excite the β and α chromophores respectively (Fig. 1c). In SM2P, the first saturating pulse drives damped Rabi oscillations between the ground state ($|0\rangle$) and the initially excited state ($|1\rangle$), resulting in an equal probability of population in both states after interaction with the pulse. Population in $|1\rangle$ relaxes to the off-resonance state ($|2\rangle$) with a timescale determined by the microscopic properties of the sample. The second saturating pulse drives the same Rabi oscillations between $|0\rangle$ and $|1\rangle$, but does not interfere with population out of resonance (*i.e.*, in $|2\rangle$). On timescales longer than the relaxation time (Fig. 1a, right), the second Rabi oscillation provides another opportunity to populate $|1\rangle$ and subsequently transfer to $|2\rangle$, increasing the population and thus fluorescence from $|2\rangle$. By detecting fluorescence from $|2\rangle$ and scanning the delay from negative to positive times, an SM2P trace is recorded that shows a dip-like shape, which can be fit to extract the timescale of energy relaxation between states.

Representative SM2P traces are shown for primarily β excitation at 610 nm (Fig. 1d,e) and primarily α excitation at 645 nm (Fig. 1f,g). While these β-excitation traces exhibit timescales that are not statistically different (148$\pm$15 and 225$\pm$70 fs in Fig. 1d and e, respectively), the α-excitation traces differ significantly (371$\pm$46 and 185$\pm$39 fs in Fig. 1f and g, respectively), providing an initial demonstration of the ability of SM2P to uncover heterogeneity in ultrafast dynamics.

Energy transfer in APC

In APC, rapid energy transfer occurs within the chromophore dimers [26]. Energy transfers from the higher energy β chromophore to the lower energy α chromophore, and so can be studied using the β excitation data. While slower (picosecond) energy transfer also occurs between dimers, it is outside the timescale measured here. Along with energy transfer, both chromophores undergo energetic relaxation on a similar timescale due to nuclear motion. SM2P measures the overall energy relaxation timescale, which includes both energy transfer and energetic relaxation. Under the high excitation fluences of SM2P, the chromophores photodegrade into quenching radical cations that decrease the fluorescence lifetime. Photodegradation generally begins on the lower energy α chromophore, likely because it

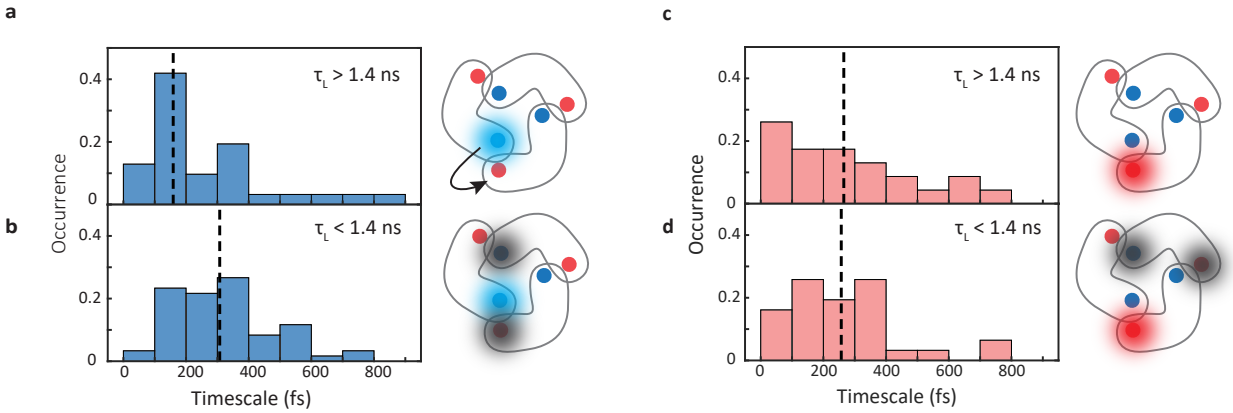

Figure 2: Distributions of energetic relaxation and energy transfer timescales for APC. Histograms of the energy relaxation timescales were constructed from the β excitation data (λ_{exc}=610 nm, blue) for the (**a**) bright (τ_L >1.4ns) population and (**b**) quenched (τ_L >1.4ns) population and from the α excitation data (λ_{exc}=645 nm, red) for the (**c**) bright population and (**d**) quenched population. The median values of the distributions are indicated by the dashed lines. As shown in (**a**), excitation of the β chromophore (blue) leads to energy transfer to the α chromophore (red). As shown in (**b**, **d**), photobleaching of individual leads to a loss of photoactivity and/or conversion into quenchers (dark gray).

remains excited for longer than the β chromophore due to the relatively long time between energy transfer and fluorescence emission [29, 30]. The negligible oscillator strength and/or spectral shifts of the photodegraded chromophore eliminate the rapid β to α energy transfer, and so only energetic relaxation due to nuclear motion remains [29, 30, 33, 34].To separate and characterize energy transfer and energetic relaxation, four histograms were constructed from the measured timescales, divided by the excitation wavelength and the concomitantly measured fluorescence lifetime. The histograms are shown in Fig. 2 for β excitation (a,b) and α excitation (c,d) for bright (τ_L >1.4 ns) and quenched (τ_L <1.4 ns) populations, respectively. Statistical parameters for the histograms are given in Table S3 in SI Section 5. The 1.4 ns cut off value was selected to separate the photodegraded APC based the fluorescence lifetime distributions (Fig. S6, SI Section 4), consistent with previous work [29, 30, 34].

In the β excitation data, the histograms have medians of 168 fs for bright APC and 308 fs for quenched APC (Fig. 2a, 2b). Comparison of the two distributions with a permutation test yielded a p-value of 0.0001 (SI Section 5.4), which establishes with a high probability (99.99%) that the two distributions are different. In contrast, in the α excitation data, the histograms have medians of 276 fs for bright APC and 257 fs for quenched APC (Fig. 2c, 2d), and comparison of the two distributions showed that they are the same (p>0.05, SI Section 5.4). Similarly, the quenched populations for β excitation and α excitation were the same (p>0.05, SI Section 5.4). In agreement with these results, only energetic relaxation is thought to be present for all three of these populations. The statistically significant shorter median

timescale for the bright population of the β excitation data, the only histogram in which energy transfer is expected, is consistent with this picture. Collectively, these results establish that the bright population of the β excitation data primarily describes energy transfer whereas the other three populations primarily describe energetic relaxation, as illustrated in the right panels of Fig. 2.

The distribution of primarily energy transfer timescales shown in Fig. 2a has a median of 168 fs and a mean of 258 fs, where the difference between these two values is due to its asymmetric profile. In previous ensemble measurements, energy transfer between the two chromophores was found to occur on 220 fs and 280 fs timescales, which were speculated to correspond to different conformational states of the protein backbone [23, 24]. The mean is consistent with these values, and the $\sim$100 fs increase over the median suggests that ensemble measurements are significantly lengthened by small sub-populations with slow transfer. This observation of an asymmetric distribution suggests that traditional theories of photosynthetic energy transfer, which were primarily developed based on mean values [2, 7, 37], may be distorted by these slow sub-populations.

An asymmetric distribution of energy transfer rates can not only lengthen the average value, but also influence the functional form of measurements. Whereas a Gaussian distribution gives rise to an energy transfer process well-described by a single-exponential function, an asymmetric distribution can lead to more complex behavior, such as a stretched exponential or the bi-exponential observed previously for APC (SI Section 5.6, SI Fig. S13) [22]. Thus, instead of characterizing distinct processes, ensemble measurements of multi-exponential dynamics may arise from non-Gaussian microscopic heterogeneity, similar to the distribution of energy transfer rates measured here for APC.

The full distribution of primarily energy transfer timescales spans $\sim$65 fs to $\sim$800 fs. In ensemble measurements with high temporal resolution, sub-50 fs energy transfer was also observed [19, 21, 22]. This population is absent here, likely due to the longer pulse durations used (100-200 fs) (SI Section 5.5). The few measured timescales above $\sim$400 fs arise from the effect of Poissonian noise, which elongate the tail of SM2P distributions [38]. The lack of a significant population slower than $\sim$400 fs suggests that static conformational states of the protein do not often dramatically slow the energy transfer timescales. The effect of heterogeneity in the local protein dielectric environment on the distribution of energy transfer timescales was previously investigated theoretically. Using combined quantum chemical/molecular mechanical simulations, a $\sim$4-fold range of energy transfer times was found

for another photosynthetic light-harvesting protein, which is roughly comparable with the measured range shown in Fig. 2a [39].

Energetic relaxation in APC

Upon photoexcitation, the chromophores in APC undergo energetic relaxation (red-shifting) due to nuclear motion including intramolecular vibrational relaxation (IVR) and solvation within the protein pocket [40]. The ultrafast solvation, known as inertial solvation, involves coupling to the short-range motions of nearby amino acid side chains and solvent molecules. The collective reorganization of solvent molecules (diffusive solvation) occurs on longer timescales than the picosecond window investigated here [41]. The combined effects of IVR and solvation give rise to the Stokes shift, which moves population out of resonance with the laser pulse. This energetic relaxation can be investigated using the histograms where no energy transfer is present. For the α-excitation data, the histograms of timescales from bright (Fig. 2c) and quenched (Fig. 2d) APC have similar median values (257 fs and 276 fs, respectively), which is consistent with previous pump-probe experiments that measured a 250 fs Stokes shift [23].

The spectral dependence of the energetic relaxation can be examined by comparing the α-excitation data to the β-excitation data for quenched APC. Similar median timescales of 308 fs for the β-excitation data and $\sim$260 fs for the α-excitation data were found. Consistently, previous measurements found comparable timescales of energetic relaxation for both chromophores, although two components at 120 fs and 230 fs were observed [23]. While the median timescales are consistent with the longer of the two components, the shorter one is absent. This may be due to the coherent excitation scheme used in the ensemble measurements or the second component may be hidden in the width of the distribution [42].

Environment-dependent heterogeneity in energetic relaxation

The influence of the protein environment on the distribution of energetic relaxation timescales was investigated by comparing the distributions for APC, CPC, and Atto647N. CPC is another cyanobacterial light-harvesting protein that is homologous to an APC monomer with an additional peripheral chromophore (SI Section 3, Fig. S4) [31, 36].There are large distances between the chromophores in CPC, and so energy transfer is slower than the time window measured here [20, 43]. Therefore, only energetic

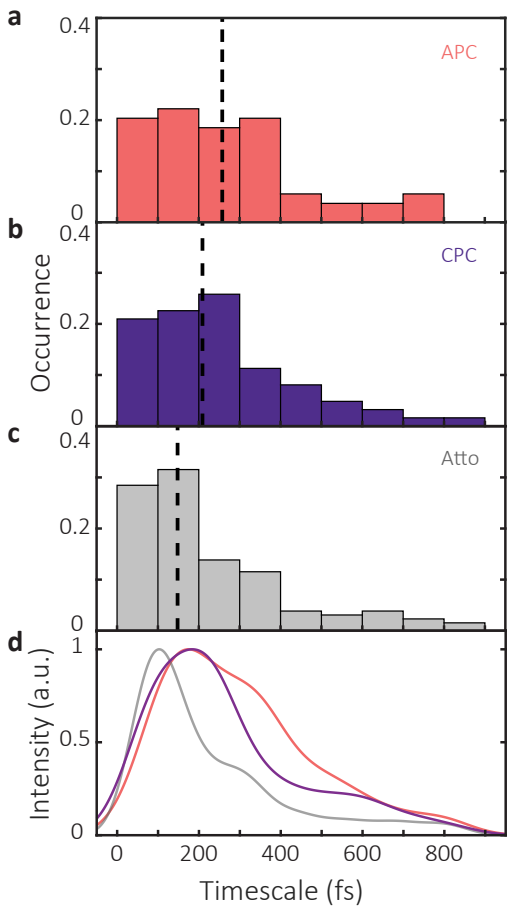

Figure 3: Comparison of histograms of energy relaxation timescales. Histograms of energy relaxation timescales for (**a**) APC with a 645 nm excitation, (**b**) CPC, and (**c**) Atto647N. The median values of each data set are marked with a dashed line at (**a**) 258 fs, (**b**) 216 fs, and (**c**) 148 fs. The kernel density estimation (KDE) smoothed fit for each histogram is shown in (**d**).

relaxation is present in the distribution. Atto647N is a widely-used single-molecule chromophore with sufficient photostability for SM2P, which the chromophores in APC and CPC lack. Histograms of the measured energetic relaxation timescales are shown in Fig. 3 for APC with α excitation (a), CPC (b) and Atto647N (c). Statistical parameters for all three distributions are given in SI Table S2, which show differences in both the peak locations and widths.

A comparison of the distribution for Atto647N to the distributions for APC and CPC isolates the contribution of a protein scaffold, as Atto647N was embedded in a polymer matrix with a local aqueous environment. The asymmetric distribution and median timescale (148 fs) for energetic relaxation of Atto647N was similar to previous measurements of other chromophores in solution. Based on the previous work, we assign the measured energetic relaxation in Atto647N to IVR with a contribution on

187 the short timescales from electronic dephasing [13, 14]. The median timescales for energetic relaxation
188 was 258 fs for APC and 216 fs for CPC. The chromophores within APC and CPC are both surrounded by
189 a protein environment, and so the slower timescales than for Atto647N suggest that the protein matrix
190 stabilizes the excited chromophore and its immediate environment to slow relaxation processes such as
191 IVR.

192 The median timescales for APC and for CPC are similar, consistent with their homologous protein struc-
193 tures. The median value for APC (258 fs) is, however, longer than for CPC (216 fs). Correspondingly,
194 the chromophores in trimeric APC (Fig. 1b) are more buried within the protein than those in monomeric
195 CPC (Fig. S4). The solvent accessible surface area (SASA) for chromophores in CPC (300 $Å^2$) is twice
196 that for chromophores in APC (150 $Å^2$). The increased solvent accessibility in CPC may create a more
197 solution-like environment that speeds up the energetic relaxation, as observed for Atto647N. Ensemble
198 ultrafast measurements compared the relaxation timescales of chromophore-containing photosynthetic
199 proteins from cryptophytes with open and closed protein scaffolds, which have correspondingly more and
200 less solvent accessibility. These measurements showed faster relaxation for the open scaffolds, consistent
201 with the results described here [44]. Other studies found that the dynamics of CPC were independent
202 of bulk solvent, initially in contradiction with a dependence of relaxation on solvent accessibility [40].
203 However, the local chromophore environment, *i.e.*, the first solvation shell, may not fully reflect changes
204 to the bulk due to interactions such as hydrogen bonding between the protein and water molecules [45].

205 In addition to differences in the median, the distributions of timescales can be used to compare the
206 heterogeneity in energetic relaxation. In SM2P, simulations have shown that the distributions are
207 extended towards longer timescales (here, values $>$500 fs) due to sampling of Poissonian-distributed
208 data [38]. To compare the heterogeneity shown in the distributions, each one was smoothed using
209 a kernel density estimation (Fig. 3d) and the full-width half maximum (FWHM) of the smoothed
210 curves was calculated, which describes the width of the main peak (SI Fig. S9). The distribution for
211 Atto647N (FWHM=179 fs) is much narrower than the distributions for APC (FWHM=462 fs) and
212 CPC (FWHM=295 fs). The width for Atto647N is similar to that measured previously for a series of
213 other chromophores in solution, where the width was ascribed to a bimodal profile from the electronic
214 dephasing and IVR contributions [13, 14, 38]. The wider distributions for APC and CPC suggest that,
215 in addition to slowing energetic relaxation, the protein matrix introduces more heterogeneity in the

relaxation timescale than is present in an aqueous solution.

The distribution of energetic relaxation timescales is also broader for APC (FWHM=462 fs) than for CPC (FWHM=295 fs). The breadth for APC may arise from increased interaction with the protein due to the more buried position of its chromophores. The distribution for APC has signatures of a bimodal structure with peaks at ∼175 fs and ∼375 fs, along with an elongated tail due to Poissonian noise as discussed above. In contrast, the distribution for CPC has only a single broad peak with a tail. The two peaks in the distribution for APC may correspond to the previously hypothesized two conformations responsible for the 220 fs and 280 fs timescales of energy transfer from ensemble measurements [22]. Alternately, previous measurements found a 400 fs component of energetic relaxation exclusively associated with the α chromophore in APC [23]. Although this component only appeared clearly upon excitation of the vibronic transition in ensemble measurements, which we do not excite here, signatures of this pathway may be contributing to the width of the measured distribution.

Discussion

In this work, we described spectrally tunable SM2P and the use of this tunability to disentangle the ultrafast dynamics of APC at the single-protein level. The distribution of primarily energy transfer timescales for APC is clustered around the median at ∼150 fs, whereas the mean — and potentially ensemble values — were lengthened due to the influence of small subpopulations. Furthermore, previous assignments of complex dynamics could instead arise from the microscopic heterogeneity, *i.e.*, non-Gaussian distribution, observed here.

Slow and heterogeneous energetic relaxation timescales for APC and CPC indicated that the protein matrix introduces variation in the photophysical processes. Because energetic relaxation is slower than energy transfer, the states involved in energy transfer are the initially excited ones, which may be how rapid energy transfer is maintained despite the effects of heterogeneous energetic relaxation. It may also be that slow energetic relaxation in the protein helps maintain vibronic coupling through an energy transfer event, which is thought to mediate rapid transfer [46]. The ability of the protein to influence the timescales of energetic relaxation means that the protein structure can control the excited states involved in energy transfer, and even the mechanism of energy transfer itself.

Methods

Single-molecule pump-probe (SM2P) spectroscopy. A schematic of the experimental setup is shown in the SI Fig. S1 and is described in detail in Ref. [38]. In brief, a tunable fiber laser (FemtoFiber pro, Toptica; 120 fs pulse duration, $\sim$4 nm bandwidth, 80 MHz repetition rate) was used as the excitation source and the laser repetition rate was reduced from 80 MHz to 2.5 MHz or 312.5 KHz with an acousto-optic pulse picker (Brimrose Corporation, FSPP-400-80-BR-800). The prism compressor was designed with single-axis translation for easy optimization with spectral maximum. The compressor was translated to minimize dispersion for each center wavelength as measured at the sample position with an interferometric autocorrelation using a GaP photodiode (Marktech, MTPD3650D-1.4) [47].Representative intensity autocorrelations for different laser excitations are shown in SI Fig. S2 with the FHWM determined assuming a Gaussian pulse. The laser pulses were split by a set of 50/50 beam splitters (Thorlabs, UFBS5050) and a delay stage in a Mach-Zehnder interferometer. The polarization was converted from horizontal to cicular polarization using a quarter-wavplate (Newlight Photonics, WPM03-Q-VIS). The excitation was coupled into a custom-designed inverted confocal microscope (Mad City labs, RM21) and focused onto the sample with an objective (UPLSAPO100XO, Olympus, NA 1.4). Fluorescence emission was collected through the same objective and separated from the excitation by use of dichroic mirrors optimized for excitation filtering (Chroma, T635lpxr-UF3; Chroma, ZT647rdc-UF2) and a pair of bandpass filters (Semrock, FF02-675/67-25; Chroma, ET690/120x) Fluorescence photons were detected on an avalanche photodiode (SPCM-AQRH-15, Excelitas) with a time-correlated single photon counting module (TimeTagger20, Swabian Instruments). Fluorescence lifetimes were fit to a single exponential decay convolved with an experimentally determined instrument response function (~ 0.5 ns) as described in SI Section 3.

For SM2P experiments, the power was set to $\sim$1 pJ/pulse before the objective or 700 $\frac{\mu J}{cm^2}$ per pulse at the sample plane. The center wavelength of the laser was tuned to either 610 nm or 645 nm. For the 610 nm measurements, experiments were performed with both near-Fourier transform limited temporal compression (118 fs) and no temporal compression (180 fs). The measured dynamics were independent of pulse duration (Fig. S7). For the 645 nm measurements, experiments were performed with no temporal compression (300 fs) due to power restraints. The delay time between the two pulses was scanned from -1.5 ps to 1.5 ps at 100 μm/s (0.33 ps/s). Fluorescence emission was binned into

50 ms bins before being fit with maximum likelihood estimation to extract energy relaxation timescales. The fit function was the convolution of the measured intensity autocorrelation with an exponential rise function for energy relaxation as detailed in SI Section 1 [13, 14, 16]. The standard error was estimated using the Fisher information matrix [48]. Single-molecule blinking and on-off transitions in SM2P traces were identified by eye and omitted from the data analysis.

Energy relaxation timescales were used to construct histograms with the bin width determined by the Freedman-Diaconis rule. The generated distributions were compared using a Permutation test, which determines the likelihood of randomly allocating the complete data-set into two groups and obtaining the experimentally observed difference (SI Section 5.2). SASA values were determined using the 'Protein interfaces, surfaces and assemblies' service PISA at the European Bioinformatics Institute located online at (http://www.ebi.ac.uk/pdbe/prot_int/pistart.html) [49].

Sample preparation. APC (Sigma Aldrich, S868), CPC, (Agilent, PB11), and Atto647N (ThermoFisher, 04507-1MG-F) were purchased and diluted to $\sim$1 nM in pH 7.4 phosphate buffer solution (ThermoFisher, AM9624). An enzymatic oxygen-scavenging system was added to the solution at final concentrations of 25 nM protocatechuate-3,4-dioxygenase and 2.5 mM protocatechuic acid [50]. The solution was spincoated in 1% PVA onto glass coverslips, which were placed on a piezoelectric stage (Mad City labs, Nano-LP100) on the microscope.

Data Availability

The data that support the findings of this study are available from the corresponding author upon request.

Acknowledgments

This work was supported by the NIH Director's New Innovator Award 1DP2GM128200-01 and a Beckman Young investigator Award (to G.S.S.-C.). R.M. acknowledges an NSF Graduate Research Fellowship. G.S.S.-C. also acknowledges a Smith Family Award for Excellence in Biomedical Research, Sloan Research Fellowship in Chemistry and a CIFAR Global Scholar Award.

Author Contributions

R.M., T.K., and G.S.S.-C. conceived and designed the experiments. R.M. and A.N. performed the experiments. R.M. and G.S.S.-C. analysed the data. R.M., A.N., and G.S.S.-C. co-wrote the paper. All authors discussed the results and commented on the manuscript.

Competing financial interests

The authors declare no competing financial interests.

References

1. Blankenship, R. E. *Molecular Mechanisms of Photosynthesis* (John Wiley & Sons, 2014).
2. Ishizaki, A. & Fleming, G. R. Unified treatment of quantum coherent and incoherent hopping dynamics in electronic energy transfer: Reduced hierarchy equation approach. *J. Chem. Phys.* **130,** 234111 (2009).
3. Ishizaki, A., Calhoun, T. R., Schlau-Cohen, G. S. & Fleming, G. R. Quantum coherence and its interplay with protein environments in photosynthetic electronic energy transfer. *Phys. Chem. Chem. Phys.* **12,** 7319–7337 (2010).
4. Novoderezhkin, V. I. & van Grondelle, R. Physical origins and models of energy transfer in photosynthetic light-harvesting. *Phys. Chem. Chem. Phys.* **12,** 7352–7365 (2010).
5. Şener, M., Strümpfer, J., Hsin, J., Chandler, D., Scheuring, S., Hunter, C. N. & Schulten, K. Förster energy transfer theory as reflected in the structures of photosynthetic light-harvesting systems. *Chem. Phys. Chem* **12,** 518–531 (2011).
6. Scholes, G. D. Long-range resonance energy transfer in molecular systems. *Annu. Rev. of Phys. Chem.* **54,** 57–87 (2003).
7. Van Amerongen, H., Valkunas, L. & van Grondelle, R. *Photosynthetic Excitons* (World Scientific, Singapore, 2000).

8. Blankenship, R. E., Tiede, D. M., Barber, J., Brudvig, G. W., Fleming, G. R., Ghirardi, M., Gunner, M. R., Junge, W., Kramer, D. M., Melis, A., Moore, T. A., Nozik, A. J., Ort, D. R., Parson, W. W., Prince R. C.and Moser, C. C., Nocera, D. G. & Sayre, R. T. Comparing photosynthetic and photovoltaic efficiencies and recognizing the potential for improvement. *Science* **332,** 805–809 (2011).

9. Lerner, E., Cordes, T., Ingargiola, A., Alhadid, Y., Chung, S., Michalet, X. & Weiss, S. Toward dynamic structural biology: Two decades of single-molecule Förster resonance energy transfer. *Science* **359** (2018).

10. Kondo, T., Chen, W. J. & Schlau-Cohen, G. S. Single-molecule fluorescence spectroscopy of photosynthetic systems. *Chem. Rev.* **117,** 860–898 (2017).

11. Beane, G., Devkota, T., Brown, B. S. & Hartland, G. V. Ultrafast measurements of the dynamics of single nanostructures: a review. *Rep. Prog. Phys.* **82,** 016401 (2018).

12. Cogdell, R. J., Gall, A. & Köhler, J. The architecture and function of the light-harvesting apparatus of purple bacteria: from single molecules to *in vivo* membranes. *Quart. Rev. Biophys.* **39,** 227–324 (2006).

13. Van Dijk, E. M., Hernando, J., Garcıa-López, J.-J., Crego-Calama, M., Reinhoudt, D. N., Kuipers, L., Garcıa-Parajó, M. F. & van Hulst, N. F. Single-molecule pump-probe detection resolves ultrafast pathways in individual and coupled quantum systems. *Phys. Rev. Lett.* **94,** 078302 (2005).

14. Van Dijk, E., Hernando, J., Garcıa-Parajó, M. & Van Hulst, N. Single-molecule pump-probe experiments reveal variations in ultrafast energy redistribution. *J. Chem. Phys.* **123,** 064703 (2005).

15. Hernando, J., van Dijk, E. M. H. P., Hoogenboom, J. P., García–López, J., Reinhoudt, D., Crego–Calama, M., García–Parajó & van Hulst, N. F. Effect of disorder on ultrafast exciton dynamics probed by single molecule spectroscopy. *Phys Rev. Lett.* **97,** 216403 (2006).

16. Malý, P., Gruber, J. M., Cogdell, R. J., Mančal, T. & van Grondelle, R. Ultrafast energy relaxation in single light-harvesting complexes. *Proc. Natl. Acad. Sci.* **113,** 2934–2939 (2016).

17. Hildner, R., Brinks, D., Nieder, J. B., Cogdell, R. J. & van Hulst, N. F. Quantum Coherent Energy Transfer over Varying Pathways in Single Light-Harvesting Complexes. *Science* **340,** 1448–1451 (2013).

18. Brinks, D., Stefani, F. D., Kulzer, F., Hildner, R., Taminiau, T. H., Avlasevich, Y., Müllen, K. & Van Hulst, N. F. Visualizing and controlling vibrational wave packets of single molecules. *Nature* **465,** 905–908 (2010).

19. Womick, J. M. & Moran, A. M. Vibronic enhancement of exciton sizes and energy transport in photosynthetic complexes. *J. Phys. Chem. B* **115,** 1347–1356 (2011).

20. Womick, J. M. & Moran, A. M. Nature of excited states and relaxation mechanisms in C-phycocyanin. *J. Phys. Chem. B* **113,** 15771–15782 (2009).

21. Womick, J. M., Miller, S. A. & Moran, A. M. Toward the origin of exciton electronic structure in phycobiliproteins. *J. Chem. Phys.* **133,** 07B603 (2010).

22. Womick, J. M. & Moran, A. M. Exciton coherence and energy transport in the light-harvesting dimers of allophycocyanin. *J. Phys. Chem. B* **113,** 15747–15759 (2009).

23. Edington, M. D., Riter, R. E. & Beck, W. F. Femtosecond transient hole-burning detection of interexciton-state radiationless decay in allophycocyanin trimers. *J. Phys. Chem. B* **101,** 4473–4477 (1997).

24. Edington, M. D., Riter, R. & Beck, W. F. Interexciton-state relaxation and exciton localization in allophycocyanin trimers. *J. Phys. Chem.* **100,** 14206–14217 (1996).

25. Edington, M. D., Riter, R. E. & Beck, W. F. Evidence for coherent energy transfer in allophycocyanin trimers. *J. Phys. Chem.* **99,** 15699–15704 (1995).

26. Beck, W. F. & Sauer, K. Energy-transfer and exciton-state relaxation processes in allophycocyanin. *J. Phys. Chem.* **96,** 4658–4666 (1992).

27. Riter, R. R., Edington, M. D. & Beck, W. F. Protein-matrix solvation dynamics in the α subunit of C-phycocyanin. *J. Phys. Chem.* **100,** 14198–14205 (1996).

28. Homoelle, B. J., Edington, M. D., Diffey, W. M. & Beck, W. F. Stimulated photon-echo and transient-grating studies of protein-matrix solvation dynamics and interexciton-state radiationless decay in α phycocyanin and allophycocyanin. *J. Phys. Chem. B* **102,** 3044–3052 (1998).

29. Goldsmith, R. & Moerner, W. Watching conformational- and photodynamics of single fluorescent proteins in solution. *Nat. Chem.* **2,** 179–185 (2010).

30. Wang, Q. & Moerner, W. Dissecting pigment architecture of individual photosynthetic antenna complexes in solution. *Proc. Natl. Acad. Sci.* **112,** 13880–13885 (2015).

31. Squires, A. H. & Moerner, W. Direct single-molecule measurements of phycocyanobilin photophysics in monomeric C-phycocyanin. *Proc. Natl. Acad. Sci.* **114,** 9779–9784 (2017).

32. Gwizdala, M., Berera, R., Kirilovsky, D., Van Grondelle, R. & Krüger, T. P. Controlling light harvesting with light. *J. Am. Chem. Soc.* **138,** 11616–11622 (2016).

33. Ying, L. & Xie, X. S. Fluorescence spectroscopy, exciton dynamics, and photochemistry of single allophycocyanin trimers. *J. Phys. Chem. B* **102,** 10399–10409 (1998).

34. Loos, D., Cotlet, M., De Schryver, F., Habuchi, S. & Hofkens, J. Single-molecule spectroscopy selectively probes donor and acceptor chromophores in the phycobiliprotein allophycocyanin. *Biophys. J.* **87,** 2598–2608 (2004).

35. Brejc, K., Ficner, R., Huber, R. & Steinbacher, S. Isolation, crystallization, crystal structure analysis and refinement of allophycocyanin from the cyanobacterium *Spirulina platensis* at 2.3 Åresolution. *J. Molec. Biol.* **249,** 424–440 (1995).

36. MacColl, R. Cyanobacterial phycobilisomes. *J. Struct. Biol* **124,** 311–334 (1998).

37. Mohseni, M., Rebentrost, P., Lloyd, S. & Aspuru-Guzik, A. Environment-assisted quantum walks in photosynthetic energy transfer. *J. Chem. Phys.* **129,** 11B603 (2008).

38. Moya, R., Kondo, T., Norris, A. & Schlau-Cohen, G. S. Spectrally-tunable femtosecond single-molecule pump-probe spectroscopy. *In Preparation.*

39. Curutchet, C., Kongsted, J., Munoz-Losa, A., Hossein-Nejad, H., Scholes, G. D. & Mennucci, B. Photosynthetic light-harvesting is tuned by the heterogeneous polarizable environment of the protein. *J. Am. Chem. Soc.* **133,** 3078–3084 (2011).

40. Homoelle, B. J. & Beck, W. F. Solvent Accessibility of the Phycocyanobilin chromophore in the α subunit of C-phycocyanin: implications for a molecular mechanism for inertial protein-matrix solvation dynamics. *Biochemistry* **36,** 12970–12975 (1997).

41. Stratt, R. M. & Cho, M. The short-time dynamics of solvation. *J. Chem. Phys.* **100,** 6700–6708 (1994).

42. Ferwerda, H. A., Terpstra, J. & Wiersma, D. A. Discussion of a "coherent artifact" in four-wave mixing experiments. *J. Chem. Phys.* **91,** 3296–3305 (1989).

43. Riter, R. E., Edington, M. D. & Beck, W. F. Isolated-chromophore and exciton-state photophysics in C-phycocyanin trimers. *J. Phys. Chem. B* **101,** 2366–2371 (1997).

44. Jumper, C. C., Arpin, P. C., Turner, D. B., McClure, S. D., Rafiq, S., Dean, J. C., Cina, J. A., Kovac, P. A., Mirkovic, T. & Scholes, G. D. Broad-band pump–probe spectroscopy quantifies ultrafast solvation dynamics of proteins and molecules. *J. Phys. Chem. Lett.* **7,** 4722–4731 (2016).

45. Biedermannová, L. & Schneider, B. Hydration of proteins and nucleic acids: Advances in experiment and theory. A review. *Biochim. Biophys. Acta Gen. Subj.* **1860,** 1821–1835 (2016).

46. Jumper, C. C., Rafiq, S., Wang, S. & Scholes, G. D. From coherent to vibronic light harvesting in photosynthesis. *Curr. Opin. Chem. Biol.* **47,** 39–46 (2018).

47. Müller, M., Squier, J. & Brakenhoff, G. Measurement of femtosecond pulses in the focal point of a high-numerical-aperture lens by two-photon absorption. *Opt. Lett.* **20,** 1038–1040 (1995).

48. Pawitan, Y. *In all likelihood: statistical modelling and inference using likelihood* (Oxford University Press, 2001).

49. Krissinel, E. & Henrick, K. Inference of macromolecular assemblies from crystalline state. *J. Mol. Bio.* **372,** 774–797 (2007).

50. Aitken, C. E., Marshall, R. A. & Puglisi, J. D. An oxygen scavenging system for improvement of dye stability in single-molecule fluorescence experiments. *Biophys. J.* **94,** 1826–1835 (2008).

Figures

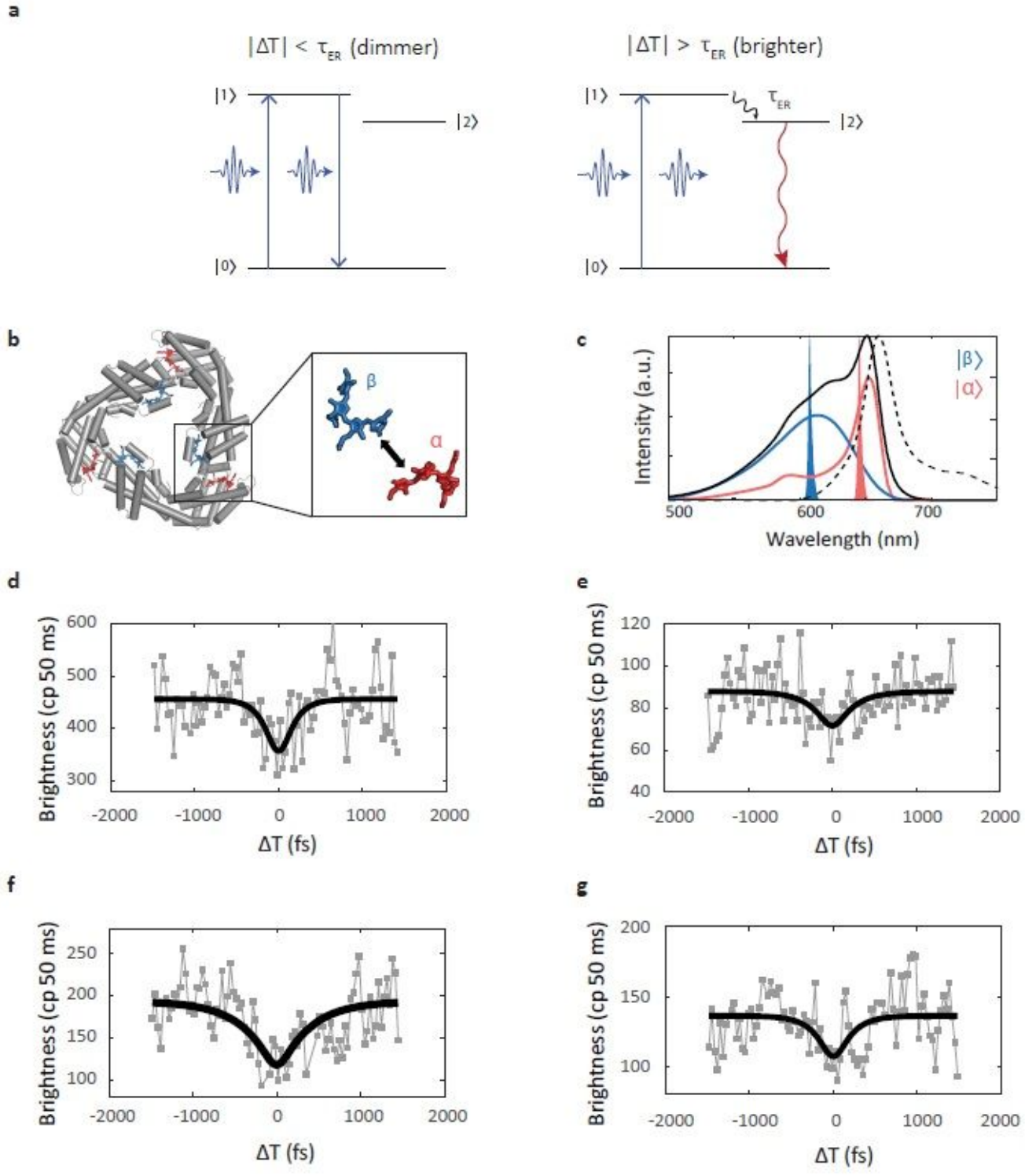

Figure 1

Single-molecule pump probe (SM2P) experiments on allophycocyanin (see Manuscript file for complete figure legend)

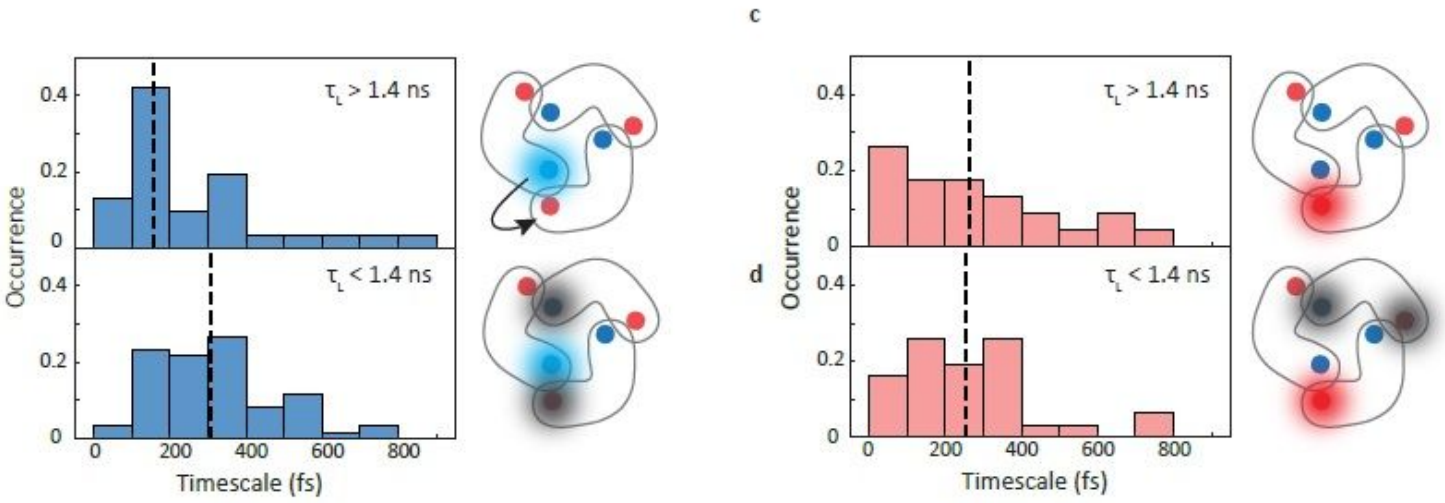

Figure 2

Distributions of energetic relaxation and energy transfer timescales for APC. (see Manuscript file for complete figure legend)

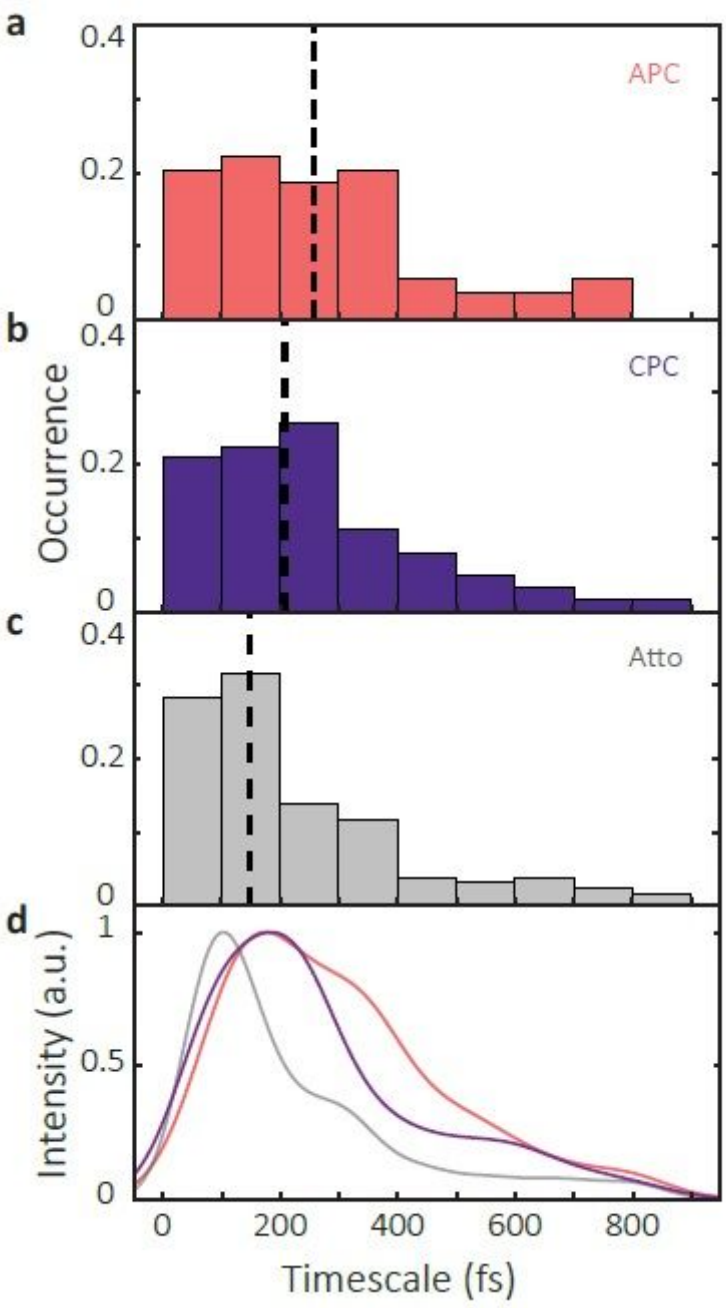

Figure 3

Comparison of histograms of energy relaxation timescales. (see Manuscript file for complete figure legend)

Supplementary Files

This is a list of supplementary files associated with this preprint. Click to download.

- MoyaAPCSIV02.pdf